

Intermediate Mass Ratio Black Hole Binaries: Numerical Relativity meets Perturbation Theory

Carlos O. Lousto, Hiroyuki Nakano, Yosef Zlochower, and Manuela Campanelli

*Center for Computational Relativity and Gravitation,
School of Mathematical Sciences, Rochester Institute of Technology,
85 Lomb Memorial Drive, Rochester, New York 14623*

(Dated: November 4, 2018)

We study black-hole binaries in the intermediate-mass-ratio regime $0.01 \lesssim q \lesssim 0.1$ with a new technique that makes use of nonlinear numerical trajectories and efficient perturbative evolutions to compute waveforms at large radii for the leading and nonleading modes. As a proof-of-concept, we compute waveforms for $q = 1/10$. We discuss applications of these techniques for LIGO/VIRGO data analysis and the possibility that our technique can be extended to produce accurate waveform templates from a modest number of fully-nonlinear numerical simulations.

PACS numbers: 04.25.Dm, 04.25.Nx, 04.30.Db, 04.70.Bw

Introduction: The dramatic breakthroughs in the numerical techniques to evolve black-hole binaries (BHB) [1–3] transformed the field and made it possible to begin constructing waveform templates for use in LIGO and VIRGO gravitational wave data analysis and detection from highly-accurate, fully-nonlinear simulations. This promises to greatly aid in the detection and analysis of gravitational waves from astrophysical sources [4].

While LISA’s sensitivity band is well suited to observe supermassive BHBs, ground based observatories are more sensitive to BHBs with masses up to a few hundred solar masses. Both of these types of BHBs are most likely to have mass ratios in the range 1:10 - 1:100 [5]. This regime is hard to model with fully-nonlinear numerical simulations, which thus far have focused on the comparable mass regime. On the other hand, BHBs in the very small mass ratio regime can, in principle, be modeled accurately with perturbation theory, and significant theoretical effort was dedicated to the consistent computation of the self-force on a point-like source orbiting around Schwarzschild and Kerr black holes (see [6] for a review of new developments in the field). These perturbative techniques allow one to formally compute geodesic deviations to second order. Although secular effects still need to be quantified, these techniques are expected to provide a good approximation for mass ratios $q = m_1/m_2 < 1/100$.

Fully-nonlinear BHB simulations with small mass-ratios are challenging and the smallest mass ratios published so far are $q = 1/10$ in the nonspinning case [7, 8] and $q = 1/8$ for highly-spinning BHBs [9]. Most fully-nonlinear numerical simulations published have been in the comparable mass regime, and consequently, most of the comparisons between NR and post-Newtonian (PN) waveforms have been in this regime (for comparisons of NR and PN waveforms from generic binaries, see [10, 11] and references therein). Similarly, phenomenological [12] and EOBNR [13] modeling of waveforms are based on

comparable-mass BHB simulations. The intermediate region of $1/100 < q < 1/10$ provides a unique opportunity to compare fully-nonlinear numerical and perturbative techniques. In this letter we introduce a novel approach to deal with this intermediate-mass-ratio regime. We perform a ‘proof of principle’ comparison, to determine an upper bound on the error in our technique, between fully-nonlinear numerical simulations and perturbative ones in the borderline case of a nonspinning BHB system with mass ratio $q = 1/10$.

The key element introduced in our approach is the use of the numerically generated trajectories (in the moving puncture approach [2, 3]) of a BHB during the late inspiral regime in a perturbative calculation of the waveform emitted by the binary.

Full Numerical Simulations: In order to approximate the late orbital parameters of a quasicircular inspiral we computed the momentum and puncture-position parameters using a resummed (particle limit) 3.5 PN evolution of a $q = 1/10$, non-spinning binary from $r = 50M$ to $r = 7.25M$. To compute the numerical initial data, we use the puncture approach [14] along with the TWOPUNCTURES [15] thorn. We chose the puncture mass parameters such that the system had a total ADM mass $M = 1$ and mass ratio $q = 1/10$.

We evolved this BHB data-set using the LAZEV [16] implementation of the moving puncture approach [2, 3]. Our code used the Cactus toolkit [17] and the Carpet [18] mesh refinement driver to provide a ‘moving boxes’ style mesh refinement. We used a modified gauge condition suggested in [19]. Our simulation used 11 levels of refinement (around the smaller components), with central resolutions as high as $M/368.64$, and 9 levels of refinement around the larger component. The outer boundaries were located at $400M$ and the resolution in the boundary zone was $h = 2.7777M$ for our finest resolution run. The BHB performs four orbits prior to merger,

TABLE I: Initial puncture data, and final remnant parameters

x_1	6.60438	x_2	-0.671518
m_1^p	8.43895×10^{-2}	m_2^p	0.907039
p_x	-3.2671×10^{-4}	p_y	4.04057×10^{-2}
M_h	0.99600	a_h	0.26081
$E_{\text{rad}} * 1000$	4.578 ± 0.684	$J_{\text{rad}}^z * 100$	3.420 ± 0.113
$V_{\text{kick}} [\text{km s}^{-1}]$	67 ± 35	t_{CAH}	$\approx 380M$

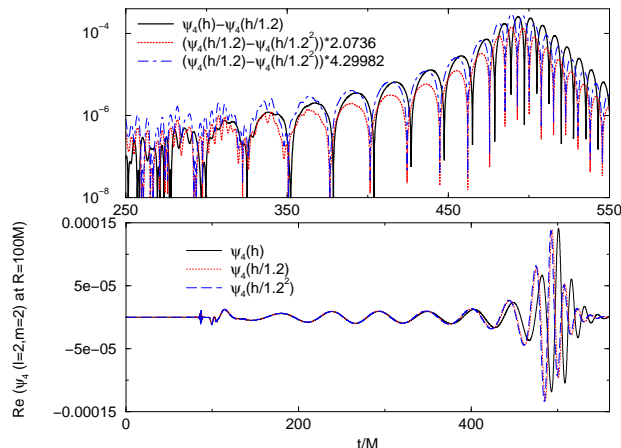


FIG. 1: Convergence of the real part of the $(\ell = 2, m = 2)$ mode of ψ_4 as computed by full numerical evolutions and extracted at $R_{\text{obs}} = 100M$. Eighth-order convergence implies $\psi_4(h) - \psi_4(h/1.2) = 4.29982(\psi_4(h/1.2) - \psi_4(h/1.2^2))$, while fourth-order convergence implies $\psi_4(h) - \psi_4(h/1.2) = 2.0736(\psi_4(h/1.2) - \psi_4(h/1.2^2))$. Initially, the error in ψ_4 is very small and dominated by grid noise, at $t \sim 250M$ the fourth-order convergence of the ψ_4 algorithm is apparent, with the convergence quickly changing to eighth-order as truncation errors in the metric and extrinsic curvature begin to dominate the errors in ψ_4 .

which occurs roughly $400M$ after the start of the simulation (see Table I).

We found that the waveform exhibits eighth-order convergence during the late-inspiral (when the errors in the waveform are dominated by phase errors associated with the orbital motion). The waveform exhibits noise which tends to mask the convergence at early times. As the simulation progresses, we first see fourth-order convergence of the Weyl scalar ψ_4 (we used a fourth-order algorithm to compute ψ_4) and later eighth-order convergence, as the errors in the waveform due to truncation errors in the metric and extrinsic curvature become important. In Fig 1 we show the convergence of the waveform during the late-inspiral. Note the very good agreement of the two finest resolution runs.

Perturbative evolutions: For the case of a nonspinning BHB in the small mass ratio regime, we can use a Schwarzschild black-hole (rather than Kerr) as the

background space-time for our perturbation expansion. This allows us to use the simpler metric perturbation equations and the Regge-Wheeler-Zerilli (RWZ) formalism [20, 21]

$$\left[-\frac{\partial^2}{\partial t^2} + \frac{\partial^2}{\partial r^{*2}} - V_\ell^{(\text{even})/(\text{odd})}(r) \right] \psi_{\ell m}^{(\text{even})/(\text{odd})}(t, r) = S_{\ell m}^{(\text{even})/(\text{odd})}[r_p(t), \Phi_p(t)], \quad (1)$$

where $V_\ell^{(\text{even})/(\text{odd})}$ denotes the Zerilli and Regge-Wheeler potentials and $S_{\ell m}^{(\text{even})/(\text{odd})}$ is the source term derived from the particle's trajectory, in the orbital plane $[r_p(t), \Phi_p(t)]$. The details are discussed in [22, 23], and we use the definitions in [24]. The consistent use of higher order tracks in this equations has been discussed in [25] (See Eq. (4.6) therein.)

The coordinates used in numerical simulations are chosen to produce stable evolutions and correspond, initially, to isotropic coordinates. Perturbative calculations, on the other hand, regularly make use of the standard Schwarzschild coordinates. The easiest way to relate the two is to translate the numerical tracks into the Schwarzschild coordinates used in Eq. (1). This can be achieved by considering the late-time numerical coordinates that correspond to radial isotropic ‘trumpet’ stationary $1 + \log$ slices of the Schwarzschild spacetime [26]. We obtain the explicit coordinate transformations following the procedure detailed in Ref. [27]. We perform the numerical integration of the perturbative equation (1) with Dirac's delta sources using the algorithm described in [22, 28].

An interesting aspect of the source term in the perturbative evolution equations (1) is that $S_{\ell m}^{(\text{even})/(\text{odd})} \rightarrow 0$ as $(1 - 2M/r_p)$ when the particle approaches the background horizon (located at $r = 2M$). This leads to essentially free evolution of the Cauchy data once the particle ‘sits’ on the horizon. In this sense perturbation theory naturally transitions to a ‘close limit’ evolution. This property means that once the black holes are close to each other, and form a common horizon, we no longer need the information of the full numerical track, since perturbation equations will describe the radiation essentially in terms of the universal quasi-normal ringing. In practice, we monitor the numerical tracks and switch off the source-terms when $r_p(t) \sim 2M$.

In Fig. 2, we plot the leading order $(\ell = 2, m = 2)$ mode of the strain h calculated both using the numerical waveform and, perturbatively, from the numerical trajectories, while in Fig. 3, we compare the nonleading $(\ell = 2, m = 1)$ and $(\ell = 3, m = 3)$ modes. The agreement between waveforms is summarized in Table II where we computed the overlap between waveforms as defined in Ref. [10]. In addition we evaluate the effects of extraction of the waveform at finite radii by extracting the perturbative waveform at $R_{\text{obs}} = 100M$ and $1000M$ and then (after a time shift) computing the overlap index (see

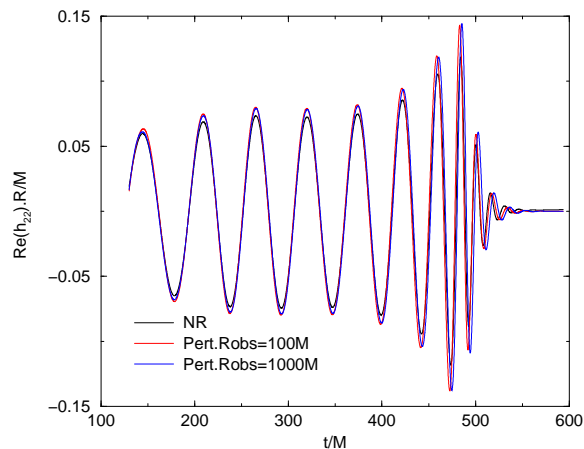


FIG. 2: The Real part of the $(\ell = 2, m = 2)$ mode of the strain h as computed by full numerical evolutions and extracted at $R = 100M$, and the corresponding perturbative evolutions for the same numerical track extracted at two radii $R_{\text{obs}} = 100M, 1000M$. The matching of the numerical and perturbative waveforms ($R_{\text{obs}} = 100M$ and $1000M$) for the whole range of evolution for $130.068 < t/M < 593.564$ are 0.987656 and 0.974751 , respectively; while for the two perturbative waveforms at different extraction radii the matching is 0.938873 .

TABLE II: The overlap (matching) of the real and imaginary parts of the modes of the strain h . The integration time is from $t/M = 130.068$ to 593.564 and the definition of the matching is given in Eqs. (26) and (27) of [10].

Mode	$\Re(\ell = 2, m = 2)$	$\Re(\ell = 2, m = 1)$	$\Re(\ell = 3, m = 3)$
Match	0.987656	0.975017	0.954138
Mode	$\Im(\ell = 2, m = 2)$	$\Im(\ell = 2, m = 1)$	$\Im(\ell = 3, m = 3)$
Match	0.987622	0.981982	0.953767

Table II). The equivalent extraction using standard numerical methods requires large computational resources, and such extractions have only recently been achieved using highly-efficient techniques such as multi-patch [29] and pseudo-spectral [30] methods.

As we mentioned, the perturbative evolution only makes use of numerical information (tracks) in the final inspiral and merger phase. After merger we have free Cauchy evolution of the perturbations. One can extend this technique to the early inspiral phase, as well. During the early-inspiral, the binary's evolution is well described by PN theory and these trajectories can be used to determine the perturbative waveforms [31]. We can thus, stitch together a 3.5PN trajectory for the inspiral phase to a full numerical evolution in the moving puncture approach. In fact, this is how we determined the initial orbital parameters for the numerical solution of General Relativity constraints to prepare full numerical evolution. The resulting waveform is shown in Fig. 4,

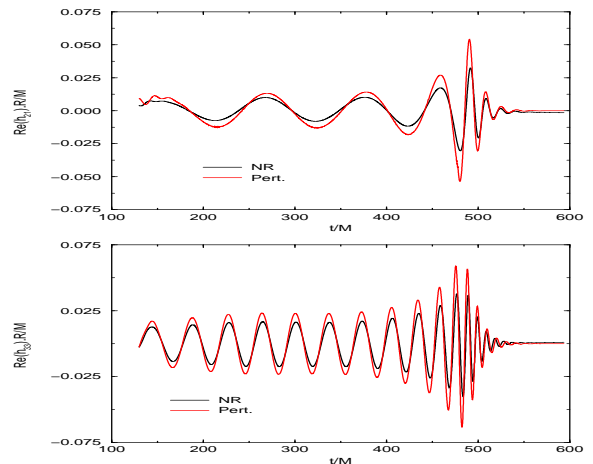


FIG. 3: Upper: The Real part of the $(\ell = 2, m = 1)$ mode of the strain h as computed by a numerical evolution and extracted at a radius $R_{\text{obs}} = 100M$, and the corresponding perturbative (odd parity) evolution for the same numerical track extracted at the same radius. Lower: The Real part of the $(\ell = 3, m = 3)$ mode of h as computed by the numerical and perturbative evolutions. Similar results are obtained for the imaginary part of the modes.

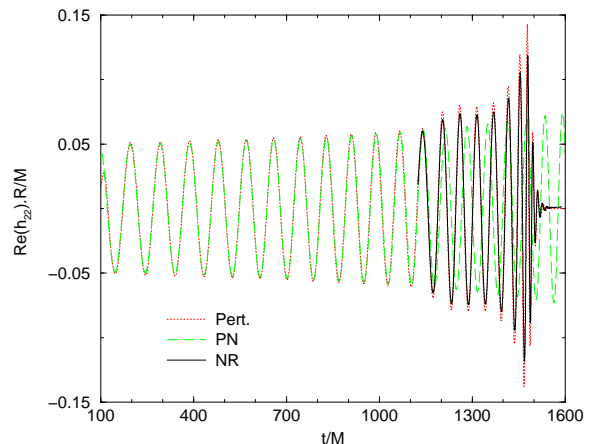


FIG. 4: The strain computed by a perturbation theory calculation of using the tracks provided by 3.5PN theory in the early-inspiral, the numerical tracks during the late-inspiral, and an effective close-limit calculation post-merger. Note that we obtain a waveform of duration $\approx 1600M$ using only the information from the first $373M$ of a fully-nonlinear numerical evolution.

which also shows the waveform produced solely with PN methods. Note that this procedure allows us to compute the complete waveform making use of numerical data from the first $t \approx 373M$ (of an over $600M$ simulation) of the numerical evolution. The procedure resembles the ‘Lazarus approach’ [32] in that it makes efficient use of numerical simulations by restricting them to the stage

of the binary evolution where they are needed.

Conclusions and Discussion: Given the current difficulties in efficiently solving the intermediate mass ratio regime by purely nonlinear numerical methods, we propose to use perturbation theory to propagate gravitational waves on a black hole background using trajectory information from a combination of nonlinear numerical and semi-analytic methods, such as the post-Newtonian approximation. In this letter we provided a ‘proof of principle’ comparison between our hybrid technique and fully nonlinear results in the most challenging case for perturbation theory, i.e. $q = 1/10$.

The benefits of this approach are apparent: i) No fitting parameters have been used in the generation of the waveforms. ii) Since perturbation equations naturally transition to close limit ones, i.e. source free wave equations, numerical tracks are not needed after merger, thus reducing the cost of the nonlinear simulations (in our example it represented a 40% reduction in running time.) iii) The perturbative evolution also provides a natural way to extract waveforms at very large radii in a well known and defined gauge, in a region accurately described by linear perturbations. Thus further cutting the size of the required numerical grid and hence the computational cost of the nonlinear simulation. iv) The computation of even, odd, leading, and higher-order modes (ℓ, m) with the same black holes trajectory. Note that the small amplitude of the non-leading terms impose additional requirements of accuracy at the extraction radii and at the external boundaries of the full numerical grid to avoid interfering reflections. v) Perturbation codes are highly efficient and run within seconds on standard CPUs, and are also amenable for running in GPUs or other accelerated hardware opening up the possibility of generating online analysis of LIGO/VIRGO data.

In order to improve the accuracy of the generated waveforms we can consider several extensions to our method. These include perturbations about a Kerr background using the Teukolsky equations [33]. In addition, adding second-order perturbative corrections [34] should improve accuracy for larger mass ratios. Finally, given our encouraging first results, one can consider a phenomenological description of intermediate-mass-ratio in-spiral trajectories based on a series of detailed nonlinear numerical runs to model the tracks of BHBs as function of mass ratio and spins. The resulting phenomenological trajectories could then be used to efficiently generate accurate waveforms over a wide region of the parameter space.

We gratefully acknowledge NSF for financial support from grants PHY-0722315, PHY-0653303, PHY-0714388, PHY-0722703, DMS-0820923, and PHY-0929114; and NASA for financial support from grants NASA 07-ATFP07-0158 and HST-AR-11763. Computational resources were provided by Ranger cluster at

TACC (Teragrid allocations TG-PHY080040N and TG-PHY060027N) and by NewHorizons at RIT.

-
- [1] F. Pretorius, Phys. Rev. Lett. **95**, 121101 (2005), gr-qc/0507014.
 - [2] M. Campanelli, C. O. Lousto, P. Marronetti, and Y. Zlochower, Phys. Rev. Lett. **96**, 111101 (2006), gr-qc/0511048.
 - [3] J. G. Baker, J. Centrella, D.-I. Choi, M. Koppitz, and J. van Meter, Phys. Rev. Lett. **96**, 111102 (2006), gr-qc/0511103.
 - [4] B. Aylott et al., Class. Quant. Grav. **26**, 165008 (2009), 0901.4399.
 - [5] M. Volonteri and P. Madau (2008), 0809.4007.
 - [6] C. O. Lousto, ed., *Special issue: Gravitational Radiation from Binary Black Holes: Advances in the Perturbative Approach*, vol. Class. Quant. Grav. **22**, S543-S868 (2005).
 - [7] J. A. Gonzalez, U. Sperhake, and B. Bruggmann, Phys. Rev. **D79**, 124006 (2009), 0811.3952.
 - [8] J. G. Baker et al., Phys. Rev. **D78**, 044046 (2008), 0805.1428.
 - [9] C. O. Lousto and Y. Zlochower, Phys. Rev. D **79**, 064018 (2009), 0805.0159.
 - [10] M. Campanelli, C. O. Lousto, H. Nakano, and Y. Zlochower, Phys. Rev. D **79**, 084010 (2009), 0808.0713.
 - [11] B. Szilagyi, L. Lindblom, and M. A. Scheel, Phys. Rev. **D80**, 124010 (2009), 0909.3557.
 - [12] P. Ajith et al. (2009), 0909.2867.
 - [13] Y. Pan et al. (2009), 0912.3466.
 - [14] S. Brandt and B. Brügmann, Phys. Rev. Lett. **78**, 3606 (1997), gr-qc/9703066.
 - [15] M. Ansorg, B. Brügmann, and W. Tichy, Phys. Rev. D **70**, 064011 (2004), gr-qc/0404056.
 - [16] Y. Zlochower, J. G. Baker, M. Campanelli, and C. O. Lousto, Phys. Rev. D **72**, 024021 (2005), gr-qc/0505055.
 - [17] *Cactus*: <http://www.cactuscode.org>.
 - [18] E. Schnetter, S. H. Hawley, and I. Hawke, Class. Quantum Grav. **21**, 1465 (2004), gr-qc/0310042.
 - [19] D. Mueller and B. Bruegmann (2009), 0912.3125.
 - [20] T. Regge and J. Wheeler, Phys. Rev. **108**, 1063 (1957).
 - [21] F. J. Zerilli, Phys. Rev. D **2**, 2141 (1970).
 - [22] C. O. Lousto, Class. Quant. Grav. **22**, S543 (2005), gr-qc/0503001.
 - [23] C. O. Lousto, Class. Quant. Grav. **22**, S569 (2005), gr-qc/0501088.
 - [24] H. Nakano and K. Ioka, Phys. Rev. **D76**, 084007 (2007), 0708.0450.
 - [25] Y. Mino, Phys. Rev. **D77**, 044008 (2008), 0711.3007.
 - [26] M. Hannam, S. Husa, D. Pollney, B. Bruggmann, and N. O’Murchadha, Phys. Rev. Lett. **99**, 241102 (2007), gr-qc/0606099.
 - [27] B. Bruggmann, Gen. Rel. Grav. **41**, 2131 (2009), 0904.4418.
 - [28] C. O. Lousto and R. H. Price, Phys. Rev. D **56**, 6439 (1997), gr-qc/9705071.
 - [29] D. Pollney, C. Reisswig, N. Dorband, E. Schnetter, and P. Diener (2009), 0910.3656.
 - [30] M. A. Scheel et al., Phys. Rev. **D79**, 024003 (2009), 0810.1767.
 - [31] A. Nagar, T. Damour, and A. Tartaglia, Class. Quant.

- Grav. **24**, S109 (2007), gr-qc/0612096.
- [32] J. Baker, M. Campanelli, and C. O. Lousto, Phys. Rev. D **65**, 044001 (2002), gr-qc/0104063.
- [33] S. A. Teukolsky, Astrophys. J. **185**, 635 (1973).
- [34] M. Campanelli and C. O. Lousto, Phys. Rev. D **59**, 124022 (1999), gr-qc/9811019.